ISIJ International, Vol. 43 (2003), No. 8, pp. 1200–1205

A Numerical Model of Rapid Solidification Processing of Ni–Al Alloy in Planar Flow Casting

Fahai BA, Gang YU[1)] and Ningfu SHEN[2)]

State Key Laboratory of Nonlinear Mechanics (LNM), Institute of Mechanics, Chinese Academy of Sciences, Beijing 100080, P.R. China. E-mail: bafahai@hotmail.com 1) Institute of Mechanics, Chinese Academy of Sciences, Beijing 100080, P.R. China. E-mail: gyu@imech.ac.cn 2) Zhengzhou University, Zhengzhou 450002, P.R. China. E-mail: Nfshen@hotmail.com

(*Received on August 26, 2002; accepted in final form on February 22, 2003*)

A numerical model has been developed for simulating the rapid solidification processing (RSP) of Ni–Al alloy in order to predict the resultant phase composition semi-quantitatively during RSP. The present model couples the initial nucleation temperature evaluating method based on the time dependent nucleation theory, and solidified volume fraction calculation model based on the kinetics model of dendrite growth in undercooled melt. This model has been applied to predict the cooling curve and the volume fraction of solidified phases of Ni–Al alloy in planar flow casting. The numerical results agree with the experimental results semi-quantitatively.

KEY WORDS: rapid solidification; numerical simulation; phase composition.

1. Introduction

Melt spinning by planar flow casting (PFC) has been widely used to produce materials with metastable or refined crystalline microstructures and to improve their properties. It is considerably important to control the solidification processing parameters in order to obtain desirable phase composition, microstructure and properties. Therefore the better understanding of the relationship between nucleation/growth kinetics and phase evolution in PFC is strongly needed. Numerous studies of the ribbon formation and solidification kinetics models have been made for PFC,[1–5)] such as modeling of crystal growth[1)] and stochastic modeling of solidification grain structure,[5)] *etc*. All works mentioned focused on heat flow characteristics and dendritic growth velocities. Few works have been reported on the kinetic analyses of multi-step solidification and the quantitative prediction of the resultant phase composition under the condition of continuous cooling from the undercooled melt, which is the case in the planar flow casting of intermetallic alloys such as Ni–Al. The purpose of the present study is to develop a numerical model, in which, the initial undercooling for the nucleation of a solid phase is determined by transient nucleation calculation, and the dendrite tip velocity at any time during the continuous cooling can be calculated by means of the BCT models. Finally, physical and mathematical models for the conversion of the S/L interface velocity to the volume fraction of the corresponding solid phase in PFC are proposed.

2. Heat Transfer Analysis

In general, the heat transfer in melt-spun ribbon is described quantitatively by a one-dimensional differential equation using a heat source term (expressed as temperature $\Delta T_{\mathrm{H.S.}}$) for the release of the latent heat of fusion as Eq. (1). For the further sake of simplicity, the whole rapidly solidified processing (RSP) is assumed to be in Newtonian cooling condition, and both the heat flow and crystal growth are unidirectional, being perpendicular to the wheel surface tangent. That is to say, no temperature gradient exists in the ribbon (solid and liquid) during the formation of crystalline ribbons in PFC. So the finite difference equation of heat transfer has only one node.

$$T_{\mathrm{a}}^{P+1}=\frac{h\cdot\Delta t}{\rho\cdot C_{\mathrm{P}}\cdot d}\cdot T_{\mathrm{w}}+\left(1-\frac{h\cdot\Delta t}{\rho\cdot C_{\mathrm{P}}\cdot d}\right)\cdot T_{\mathrm{a}}^{P}+\Delta T_{\mathrm{H.S.}} \quad ...(1)$$

where h – heat transfer coefficient in the wheel/alloy contact interface, Δt – time interval, ρ – the average density of melt, C_{P} – the average specific heat of melt; d – the thickness of ribbon, T_{w} – the substrate temperature (=298 K), T_{a}^{P+1} – the node temperature of the alloy ribbon in P+1 time step, $\Delta T_{\mathrm{H.S.}}$ – the node temperature of the alloy ribbon in P time step, T_{a}^{P} – the temperature increase in the ribbon resulted from the latent heat releasing of relating crystal growth volume fraction.

$$\Delta T_{\mathrm{H.S.}}=\frac{\Delta V\cdot\Delta H_{\mathrm{V}}}{C_{\mathrm{P}}} \quad .....(2)$$

where ΔH_{V} – the latent heat of fusion per unit volume; ΔV – the volume increase of solid in a time step.

Boundary conditions: The temperature of copper wheel always keeps at (T_{w}) 298 K in PFC; the node temperature is equal to that of the starting melt when t=0.

3. Nucleation and the Initial Nucleation Undercooling (the Initial Nucleation Temperature)

The initial nucleation temperature is a sign temperature of starting solid–liquid transformation. When the total volume of nuclei accumulates up to 10^{-6} within a unit volume in PFC, This temperature (expressed as T_N) is referred to as initial nucleation temperature. At T_N point, the melt has a maximum of undercooling ΔT_{max}, and the solid phase has a maximum of crystal growth velocity.

$$\Delta T_{max}=T_L-T_N \quad \text{.....(3)}$$

Where T_L is liquidus temperature of alloy.

Under isothermal conditions, the time (t) dependent nucleation rate J_t is related to the steady state nucleation rate J_s by[6]:

$$J_t=J_s\left[1+2\sum_{m=1}^{\infty}\frac{(-1)^m}{m^2}\cdot\exp(-m^2t/\tau)\right] \quad \text{.....(4)}$$

Where J_t is transient nucleation rate, J_s is the steady state nucleation rate, τ is the time lag. The time dependence of transient nucleation rate, when plotted as J_t/J_s *versus* t/τ shows that $t>5\tau$, J_t reaches 99% of the steady state value J_s. Conseqently we can consider that after the transient time 5τ (also referred as the incubation time) the steady state nucleation rate is achieved. In Solid/Liquid transformations this time is extremely small and difficult to detect. In condensed systems the transient time is generally much longer and it can be observed. In these systems it is important to take account of the transient t nucleation behavior in interpreting transformation kinetics.

When the melt temperature is below the alloy liquidus temperature, the critical nuclei number (Nt) formed can be expressed as Eq. (5) within a time interval t ($=\Delta t$ in Eq. (1), provided that t is small enough to the temperature field calculation, T is a constant).

$$Nt=\int_0^t J_t\cdot dt=J_s\left[t-\frac{\pi^2\tau}{6}-2\tau\sum_{m=1}^{\infty}\frac{(-1)^m}{m^2}\cdot\exp(-m^2t/\tau)\right] \quad \text{.....(5)}$$

When $t<5\tau$ transient nucleation becomes important. In the transient regime the nucleation rate is dependent on the cluster size at which it is "measured". The larger the size the longer the transient time. The time τ for heterogeneous nucleation in undercooled alloy melts was previously derived as[7]:

$$\tau=\frac{1}{5}\cdot\frac{7.2Rg\cdot f(\theta)}{1-\cos\theta}\cdot\frac{a_0^4}{d_a^2\cdot X_{L,eff}}\cdot\frac{T_r}{D_L\cdot\Delta S_m\cdot\Delta T_r^2} \quad \text{...(6)}$$

$$J_s=\frac{N_v d_a^2 X_{L,eff}(1-\cos\theta)D_L\cdot\sigma_m^{1/2}}{a_0\sqrt[4]{f(\theta)RgT}}\cdot\exp\left[-\frac{16\pi\alpha^3 f(\theta)}{3Rg}\cdot\frac{\Delta S_m}{\Delta T_r^2\cdot T_r}\right] \quad \text{.....(7)}$$

Where Rg is the gas constant, a_0 is the atom jump distance, d_a is the average atom diameter of the solid phase, θ is the wetting angle, $f(\theta)=1/4\cdot(2-3\cdot\cos\theta+\cos\theta^3)$, ΔS_m is the entropy of fusion, D_L is the solute atom diffusivity in the undercooled melt, $X_{L,eff}$ is the effective alloy concentration, $T_r=1-\Delta T_r$, $\Delta T_r=T/T_m$, T_m is the melting point of the solidifying phase, T is the melt temperature at any time step in RSP ($T=T_a^{P+1}$, decided by Eq. (1), the same in following equations), N_v is the number of potent heterogeneous nucleation site of liquid, α is the construction factor, σ_{LS} is the interface energy per unit area between solid and liquid, σ_m is the mole interface energy between solid and liquid.

According to classical nonhomogeneous nucleation theory, when the nuclei is starting to form from liquid, the system Gibbs free energy can be written as

$$\Delta G=\frac{4}{3}\pi r^3\Delta G_{LS}f(\theta)+4\pi r^2\sigma_{LS}f(\theta) \quad \text{.....(8)}$$

Where ΔG_{LS} is solid/liquid Gibbs free energy difference per unit volume. Assuming $d\Delta G/dr=0$, the critical nuclei radius r^* is obtained

$$r^*=-\frac{2\sigma_{LS}}{\Delta G_{LS}} \quad \text{.....(9)}$$

Equation (9) may be substituted into Eq. (8), to obtain the critical nucleation work

$$\Delta G^*=\sigma_{LS}\cdot\frac{4}{3}\pi(r^*)^2\cdot f(\theta) \quad \text{.....(10)}$$

Where r^* is the critical radius of nuclei at a certain temperature T.

And the critical nucleation work can also be expressed as Eq. (11) in RSP[8]

$$\Delta G^*=\frac{16\pi\alpha^3 f(\theta)}{3Rg}\cdot\frac{\Delta S_m(T)}{\Delta T_r^2 T_r}\cdot K_B T \quad \text{.....(11)}$$

Where K_B is boltzman constant.

Therefore r^* can be given out from Eqs. (10) and (11)

$$r^*=\sqrt{\frac{4\alpha^3}{Rg\cdot\sigma_{LS}}\cdot\frac{\Delta S_m(T)}{\Delta T_r^2*T_r}\cdot K_B T} \quad \text{.....(12)}$$

While nuclei volume V_i within a time interval t

$$V_i=Nt\cdot\frac{4}{3}\pi(r^*)^3\cdot f(\theta) \quad \text{.....(13)}$$

The total nuclei number Nz and accumulative nuclei volume V_z, from liquidus temperature to initial nucleation temperature, may be obtained by integrating

$$V_z=\sum_{t=0}^{t=t_{T_N}}V_i=\sum_{T=T_L}^{T=T_N}\left[Nt\cdot\frac{4}{3}\cdot\pi(r^*)^3 f(\theta)\right] \quad \text{.....(14)}$$

If $V_z=10^{-6}V_l$, V_l is the residual liquid volume when the temperature reach temperature T_N for a subsequently solidifying phase, then the T_N can be solved out.

4. Melt Undercooling and Dendrite Tip Growth Velocity

During the continuous cooling, the tip growth velocity and the total puddle undercooling can be evaluated by BCT model[9,10] of dendrite growth in undercooled melt. The outline of BCT model is briefly reviewed as follows.

The total puddle undercooling of melt, ΔT, is expressed as

$$\Delta T=\frac{\Delta H_{\mathrm{v}}\,\mathrm{Iv}(P_t)}{C_{\mathrm{p}}}+\frac{2\Gamma}{r}+\frac{-m_{\mathrm{v}}C_0[k_{\mathrm{e}}-k(1-\ln(k/k_{\mathrm{e}}))]}{(1-k_{\mathrm{e}})[1-(1-k)\mathrm{Iv}(P_c)]}+\frac{v}{v_0}\frac{m}{1-k}+m_{\mathrm{v}}C_0\left[1-\frac{m_{\mathrm{v}}/m_{\mathrm{e}}}{1-(1-k)\mathrm{Iv}(P_c)}\right]+(m-m_{\mathrm{v}})c_0 \quad \text{.....(15)}$$

where P_t is the thermal Peclet number, P_c is the solutal Peclet number, Iv( ) is Ivantsov function, Γ is the Gibbs–Thompson coefficient, r is the dendrite tip radius, C_0 is the solute concentration, v and v_0 are growth rate and the upper limit rate of interface advance (as to intermetallic compounds: $v_0=D_i/a_0$, D_i (1–20×10^{-10} m^2/s) is the interface diffusion coefficient), k and k_{e} are nonequilibrium and equilibrium solute partition coefficients, m_{e} is the equilibrium liquidus slop, m_{v} is the nonequilibrium liquidus slope and this is given by[11]

$$m_{\mathrm{v}}=m_{\mathrm{e}}\left(1+\frac{k_{\mathrm{e}}-k+k\ln(k/k_{\mathrm{e}})}{1-k_{\mathrm{e}}}\right) \quad \text{.....(16)}$$

And the growth rate dependent partition coefficient, k, can be written as

$$k=\frac{k_{\mathrm{e}}+v\cdot\dfrac{a_0}{D}}{1+v\cdot\dfrac{a_0}{D}} \quad \text{.....(17)}$$

Tip radius of a growing dendrite, r, is calculated using the following equation as obtained from the interface stability condition[9]

$$r=\frac{\Gamma/\sigma^*}{\dfrac{P_t\Delta H_{\mathrm{v}}}{C_{\mathrm{P}}}\xi_{\mathrm{l}}-\dfrac{2m_{\mathrm{v}}P_cC_0(1-k)}{1-(1-k)\mathrm{Iv}(P_{\mathrm{c}})}\xi_{\mathrm{c}}} \quad \text{.....(18)}$$

Where

$$\xi_{\mathrm{l}}=1-\frac{1}{\sqrt{1+\dfrac{1}{\sigma^*P_t^2}}} \quad \text{.....(19)}$$

$$\xi_{\mathrm{c}}=1+\frac{2k}{1-2k-\sqrt{1+\dfrac{1}{\sigma^*P_c^2}}} \quad \text{.....(20)}$$

Where ξ_{l} is function of thermal Peclet number, ξ_{c} is function of solute Peclet number, σ^* is stability constant (=0.025).

However, a supplementary equation is also necessary

$$\Delta T=T_{\mathrm{L}}-T \quad \text{.....(21)}$$

Where liquidus temperature, T_{L}, changing with residual melt chemical composition in solidification.

The Eq. (21) describes the amount of puddle undercooling in undercooled melt, determined by heat transfer calculation and chemical composition of the remnant liquid.

Dendrite tip growth velocity and puddle undercooling at an arbitrary puddle temperature during continuous cooling, can be obtained from Eqs. (15)–(21), which can be solved by iteration method.

5. Physical and Mathematic Models of the Solid Phase Volume Fraction Evaluation

Assuming that the temperature field and the dendrite tip velocity remain stable in a time step Δt and the undrecooling and tip growth velocity are same for each dendrite of the same phase, the following assumptions can be further proposed:

- A proportion relation exists between the dendrite tip growth velocity in radial and axial directions. While the axial velocity is increasing, the radial velocity is also increasing, even though they are not equal to each other.
- Dendrite root transaction is regarded as the macroscopical reference site of solid-liquid interface and the solid volume fraction increment equals to the interface advance (see **Fig. 1**.).

Based on the above assumptions, A_j, the dendrite root transaction area of j phase related to an unit wheel/alloy contact interface area in the macroscopical reference solid-liquid interface, can be calculated as

$$A_j=\frac{v_j^2}{\sum_1^N v_j^2} \quad \text{.....(22)}$$

Where v_j is the dendrite tip growth velocity of j phase, N is the number of growing phases. However whether multi-phases competition growing exists can be judged by undercooling from the Eq. (18).

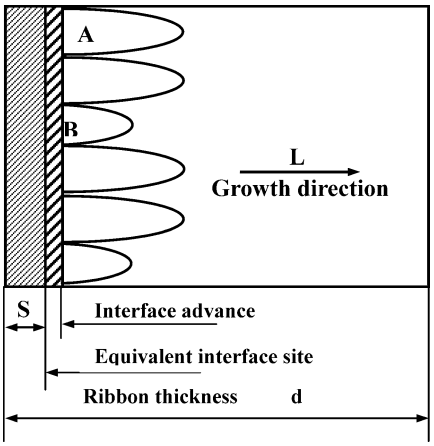

Fig. 1. The physical model of dendrite growth in undercooling melt.

The solid volume increment of j phase, ΔV_j, related to an unit wheel/alloy contact interface area in a Δt time step, can be obtained

$$\Delta V_j = A_j \cdot v_j \cdot \Delta t \quad \text{.....(23)}$$

The volume of j phase solidified in a time or temperature range is expressed as

$$VZ_j = \sum_0^t \Delta V_j = \sum_{T_L}^T \Delta V_j \quad \text{.....(24)}$$

The total solid volume (*Volz*) of various phases in a multi-step solidification

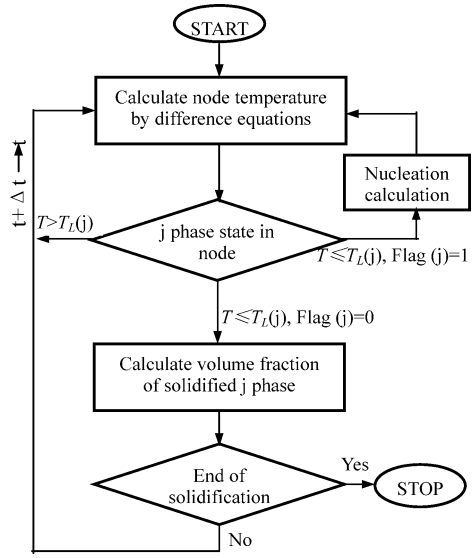

Fig. 2. Flow diagram for numerical calculation model.

$$Volz = \sum_1^j VZ_j \quad \text{.....(25)}$$

The melt state of unit node can be judged based on the calculated melt temperature profile and undercooling of a certain phase. When the melt temperature is less than the liquidus temperature of a certain phase (such as j phase), the j phase starts to nucleate. It is obvious that a certain undercooling is necessary for nucleation. When the total volume of j phase nuclei accumulates up to 10^{-6} within an unit volume, the j phase starts to grow with a certain growth velocity determined by the undercooling using BCT model, and a sign function flag (j) will be assigned as zero in program. It is no doubt that the phase selection and subsequent competitive growth exists in RSP. However, the solidified phase sequence is decided by nucleation competition, and the volume fraction by growth competition relating to undercooling. The series of calculation will be repeated until the end of solidification, as shown in **Fig. 2**.

6. Numerical Results and Analysis

The present model was applied to simulate the rapid solidification process of $Ni_{31.5}Al_{68.5}$ alloy ribbon with a complicated multi-step solidification behavior. Computational results were compared with those obtained experimentally. In the ribbon production by PFC technique a copper wheel of 350 mm in diameter was used, the crucible and nozzle were made of quartz. The initial temperature of the melt was 1 723 K, and the wheel surface kept at 298 K during the experiment.

The parameters and thermal-physical properties used in the simulation are shown in **Table 1**. The simulating pro-

Table 1. Thermophysical data used in the computation.

Parameters	$NiAl_3$	Ni_2Al_3	NiAl	References
ΔS_m: Entropy of fusion (J/mol • K)	13.98	14.13	13.46	
ΔH_m: Heat of fusion (J/mol)	9983	1054	62720	
C_P: Specific heat (J/mol • K)		40		13)
α_l: Thermal diffusivity (• $10^{-6}m^2/s$)		5		13)
σ_{LS}: S/L interface energy (J/m^2)	0.27	0.24	0.35	13)
σ_m: Mole interface energy (J/mol)	9568	8322	13920	
k_e: Equilibrium Partition coefficient	1.34	1.27	1.3	
a_0: Atom jump distance (• 10^{-9}m)	1	2	1	13)
T_m: Melting temperature (K)	1158	1408	1913	
α: Structure factor	0.6	0.52	0.87	
d_a: Average atom diameter of solid phase (• 10^{-10}m)	2.44	2.4	2.391	
D: Interface diffusion coefficient (m^2/s)	$5 \cdot 10^{-10}$	$7.5 \cdot 10^{-10}$	$8 \cdot 10^{-10}$	
v_0: Upper limited growth velocity of interface advance (m/s)	2	3	1	
$X_{L,eff}$: effective alloy concentration	0.77	0.96	0.91	
Γ:Gibbs-Thompson coefficient (mK)		$2.8 \cdot 10^{-7}$		14)
ρ: Solid density (g/cm^{-3})	3.98	4.79	5.86	
m_e: Liquidus slope (K/at.%)	10	14.5	45	
N_V: the number of potent nucleation site per volume liquid ($1/cm^3$)		$5 \cdot 10^{16}$		8)

Note : These data, for which original sources are not indicated, are from the present computation

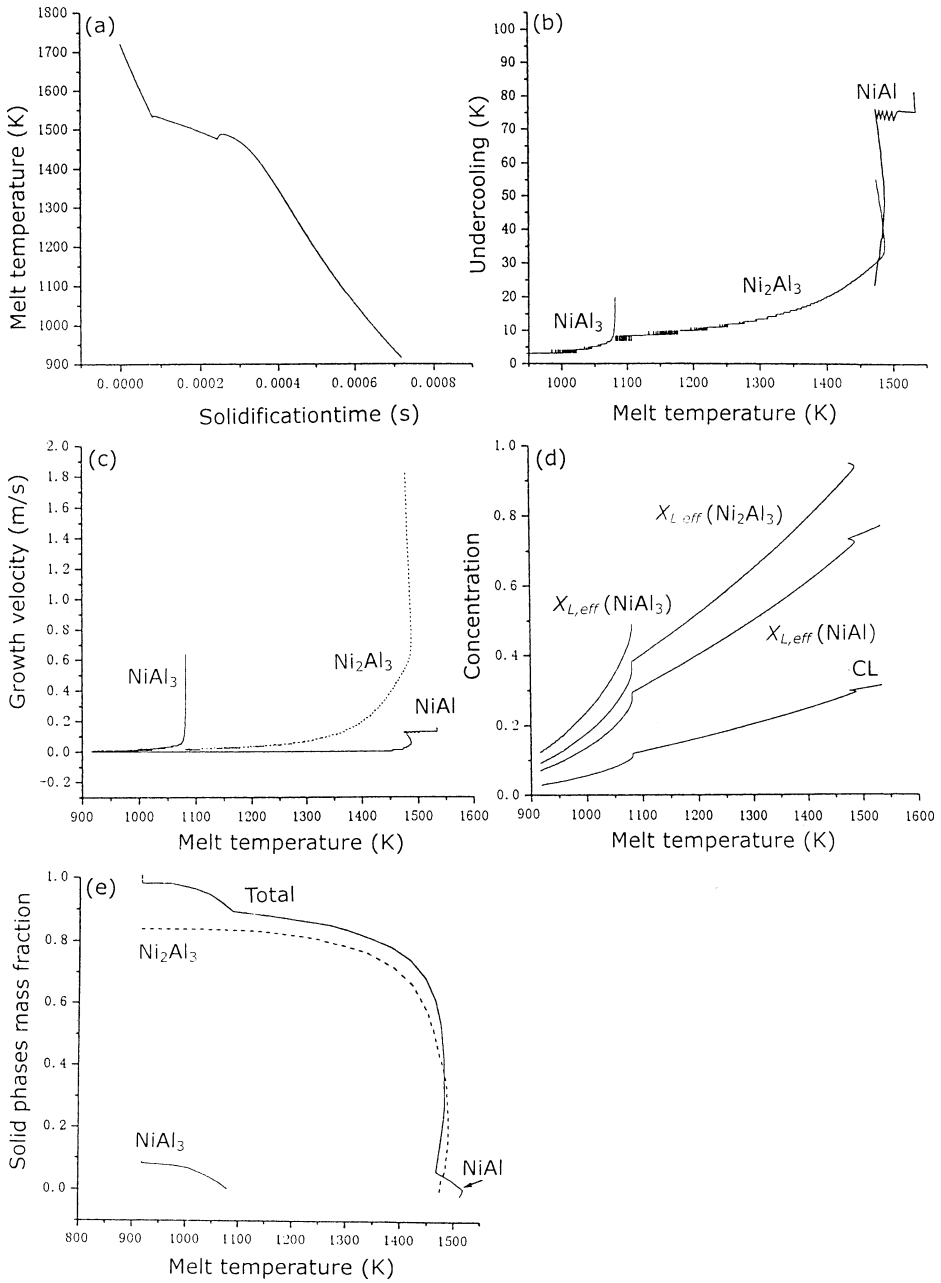

Fig. 3. Computational simulation of the solidification process and phase composition of rapidly solidified $Ni_{31.5}Al_{68.5}$ alloy ribbon with the thickness of 100 μm.

Table 2. Numerical simulation results of $Ni_{31.5}Al_{68.5}$ alloy ribbons.

Ribbon thickness (μ m)	Wetting angle	Initial nucleation temperature T_N (K)	Phase component (wt. %)			
	θ ($^\circ$)	Nail/ Ni_2Al_3/ $NiAl_3$	NiAl	Ni_2Al_3	$NiAl_3$	α -Al
100	44/36/38	1518/1490/1079	6	84	8	2
100		Experimental results	4	84	10	2

Note: The selected values of heat transfer coefficients were 60w/cm^{2}k and 15w/cm^{2}k before and after the start of solidification, respectively[11].

cessing is shown in **Figs. 3**(a)–3(e), where the changes of kinetic parameters (such as undercooling, effective alloy concentration, *etc*.) and the volume fractions of subsequently solidified intermetallic compound phases are indicated. The comparison between simulated results and experimental results is shown in **Table 2**, the calculated phase composition is in good agreement with those obtained experimentally.

The calculated temperature profile in Fig. 3(a) describes the solidification processing of a 100 μm thick ribbon of the experimental Ni–Al alloy. The first and the second inflexions indicate the initial nucleation temperature (T_N) of the

primary and the second phases in RSP, respectively. It means that NiAl phase starts to change from a liquid to solid state at 1 518 K, and the nucleation temperature range calculated is from 1 603 K (liquidus temperature) to 1518 K. While that for Ni_2Al_3 is from 1 545 to 1 490 K. NiAl is a primary phase, Ni_2Al_3 is second phase, and nucleation competition always exists in above temperature scope (1 545–1 518 K). The T_N for $NiAl_3$ is 1 079 K, but the inflexion is not shown in the Fig. 3(a), it will be explained in following parts. When the melt temperature reaches the initial nucleation temperature, the primary phase (such as NiAl) occurs, the interface contact mode between melt and wheel surface is changed from a tight contact to a mechanical contact, leading to dramatic decreasing of the heat transfer coefficient.[11] With the latent heat released into melt, the melt temperature began to go up. High cooling rate and low growth velocity lead to a faint temperature recalescence in the initial stage. When the melt temperature reaching the initial nucleation temperature of the second phase (Ni_2Al_3), the growth of competing phases cannot be avoided between the primary phase (NiAl) and second phase (Ni_2Al_3) in the undercooling melt. Faster growth (see also Fig. 3(c)) leads to a large amount of latent heat release, so the melt reaches a higher temperature in a shorter time. As a result, an obvious recalescence forms. In comparison with that of solidifying stage of NiAl and Ni_2Al_3, the temperature recalescence is not happening at $NiAl_3$ growing stage. According to the Ref. 12), the heat transfer velocity become much faster, and the residual liquid volume is very little, so the cooling rate increases fast in the last stage of solidification.

Figure 3(b) indicates the changes of undercooling for different phases. The initial undercooling of NiAl phase approaches to 85K. The fluctuation of the undercooling shows the relative change of the latent heat released and the heat transfer out to substrate.

Figure 3(c) indicates the changes of growth velocity with the melt temperature for different phases. At T_N point, a larger growth velocity exists in comparison with that in other temperature range. Multi-phase growth competition is also shown, but the competition is limited in a small temperature range. The chemical composition of melt for intermediate phases decrease very fast with solidifying (see Fig. 3(d)), leading liquidus temperature decrease fast for intermediate phases, therefore the undercooling is becoming small. As a result, the growth velocity decrease of phases with solidifying. This is a not same as isothermal computing results[12].

Figure 3(d) indicates the changes of effective alloy concentrations of different phases with melt temperature, which has an important effect on crystal growth of different phases in undercooled melt.

Figure 3(e) depicts the solid phase volume fractions vs. melt temperature, showing the solidification sequence. NiAl is the primary phase, Ni_2Al_3 is the second phase, and $NiAl_3$ is the final phase. The final stage is eutectic. As a result, the change of volume fractions of different phases in whole temperature range of multi-step solidification is described quantitatively.

A comparison has been made between numerical results and experimental measurements as shown in Table 2. It shows that the present model can describe the kinetic process of multi-step solidification of intermetallic alloys. However, it should be pointed that the fitness between calculation and experiment depends on the correct selection of all parameters. From this point of view, the present model is only a semi-quantitative method in numerical simulation of multi-step rapid solidification and resultant phase composition.

7. Conclusion

Based on the one-dimensional Newtonian heat transfer model in the direction of ribbon thickness, transient nucleation theory and BCT model, a new numerical method was developed for quantitative simulation of the resultant phase composition during RSP. Physical and mathematical models were set up by the integration of the nucleation and crystal growth in the whole temperature range of multi-step solidification of various phases, as well as for the conversion to the volume fractions of the phases in the entire microstructure. The numerical simulation results for the $Ni_{31.5}Al_{68.5}$ alloy agreed with the experimental analyses satisfactorily.

Acknowledgments

The authors gratefully acknowledge the financial support of the China State Nature Science Foundation (contract No. 59771033).

REFERENCES

1) S. A. Berger and D. K. Al: *Metall. Trans*., **19B** (1988), 571.
2) L. Gránásy: *Trans. Jpn. Inst. Met*., **27** (1986), 51.
3) K. Takeshita and P. H. Shingu: *Trans. Jpn. Inst. Met*., **27** (1986), 141
4) Z. Gong, P. Wilde and E. F. Matthys: *Int. J. Rapid Solidif*., **6** (1991), 1.
5) K. Y. Lee and C. P. Hong: *ISIJ Int*., **37** (1997), 38.
6) D. Kashchiev: *Surf. Sci.*, **14** (1969), 209.
7) G. Shao and P. Tsakiropoulos: *Acta Metall. Mater*., **42** (1994), 2937.
8) N. Saunders and P. Tsakiropoulos: *Mater. Sci. Technol*., **4** (1988), 157.
9) R. Trivedi and W. Kurz: *Int. Mater. Rev*., **39** (1994), 49.
10) G. D. Alfred and A. Teiichi: *Metall. Mater. Trans. A*, **29A** (1998), 3047.
11) K. Takeshita and P. H. Shingu: *Trans. Jpn. Inst. Met*., **27** (1986), 454.
12) F. H. Ba and N. F. Shen: *Acta Metall. Sin*., **37** (2001), 846.
13) M. Barth, B. Wei and D. M. Herlach: *Mater. Sci. Eng. A*, **A226**–**228** (1994), 770.
14) O. Hunziker and W. Kurz: *Metall. Mater. Trans. A*, **30A** (1999), 3167.